Molecular Reorganization in Organic Field-Effect Transistors and Its Effect on Two-Dimensional Charge Transport Pathways

Fabiola Liscio,[†] Cristiano Albonetti,[‡] Katharina Broch,[§] Arian Shehu,[‡] Santiago David Quiroga,[‡] Laura Ferlauto,[†] Christian Frank,[§] Stefan Kowarik,[⊥] Roberto Nervo,[¶] Alexander Gerlach,[§] Silvia Milita,[†,*] Frank Schreiber,[§] and Fabio Biscarini[‡,*]

[†]CNR—Istituto per la Microelettronica e Microsistemi (IMM), I-40129 Bologna, Italy, [‡]CNR—Istituto per lo Studio dei Materiali Nanostrutturati (ISMN), I-40129 Bologna, Italy, [§]Institut für Angewandte Physik, Universität Tübingen, Auf der Morgenstelle 10, D-72076 Tübingen, Germany, [⊥]Institut für Physik, Humboldt-Universität zu Berlin Newtonstrasse 15, D-12489 Berlin, Germany, and [¶]ESRF, 6 rue Jules Horowitz, BP 220 38043 Grenoble, France

ABSTRACT Charge transport in organic thin film transistors takes place in the first few molecular layers in contact with the gate dielectric. Here we demonstrate that the charge transport pathways in these devices are extremely sensitive to the orientational defects of the first monolayers, which arise from specific growth conditions. Although these defects partially heal during the growth, they cause depletion of charge carriers in the first monolayer, and drive the current to flow in the monolayers above the first one. Moreover, the residual defects induce lower crystalline order and charge mobility. These results, which are not intuitively explained by electrostatics arguments, have been obtained by combining *in situ* real time structural and electrical characterization together with *ex situ* AFM measurements, on thin films of a relevant n-type organic semiconductor, *N*,*N*′-bis(*n*-octyl)-dicyanoperylene-3,4:9,10-bis dicarboximide grown by sublimation in a quasi-layer-by-layer mode at different substrate temperatures.

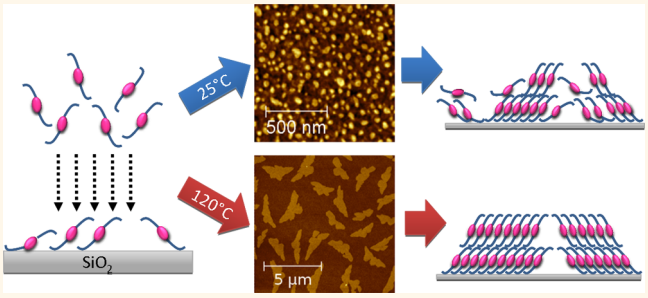

KEYWORDS: thin film growth · molecular organization · organic field-effect transistors · organic electronics · perylene derivatives

Sublimation of π-conjugated molecules in high vacuum is technologically important for growing active thin films in organic field effect transistors (OFETs). In such devices the charge transport is confined within the first few monolayers grown on the gate dielectric,[1−7] and it is two-dimensional (2D) in stacked molecular layers.[8] The number of active molecular layers and the distribution of charge carriers across the stack may vary depending on the growth rate.[7]

Molecular thin film growth is far more complex than atomistic growth described by classical growth modes.[9−12] Organic semiconductor molecules have roto-vibrational degrees of freedom, anisotropic shape, and intermolecular interactions governed by dispersive forces. As high-vacuum sublimation is a nonequilibrium process,[13−16] the energy barriers at the surface and in the film[17,18] determine self-affine morphology with time- and space correlations.[14]

The correlation between charge transport, molecular order, and morphology has been widely explored.[19] A still open question concerns the nature of disorder generated during the early stages of growth, and how it affects charge transport in OFETs. Domain boundaries yield rapidly varying local electrostatic potential in the channel,[8,20] causing charge trapping and modulation of charge mobility by few orders of magnitude.[21,22] Coexistence of islands of homeotropically oriented molecules and regions with a low-density layer of planar molecules was reported for sexithienyl,[23,24] its occurrence being related to surface chemistry.[25] The planar phase disappears in favor of the homeotropic orientation as growth proceeds. How these defects may affect OFET response is a matter of debate.

* Address correspondence to milita@bo.imm.cnr.it, f.biscarini@bo.ismn.cnr.it.

Received for review October 12, 2012 and accepted January 27, 2013.

Published online January 27, 2013
10.1021/nn304733w

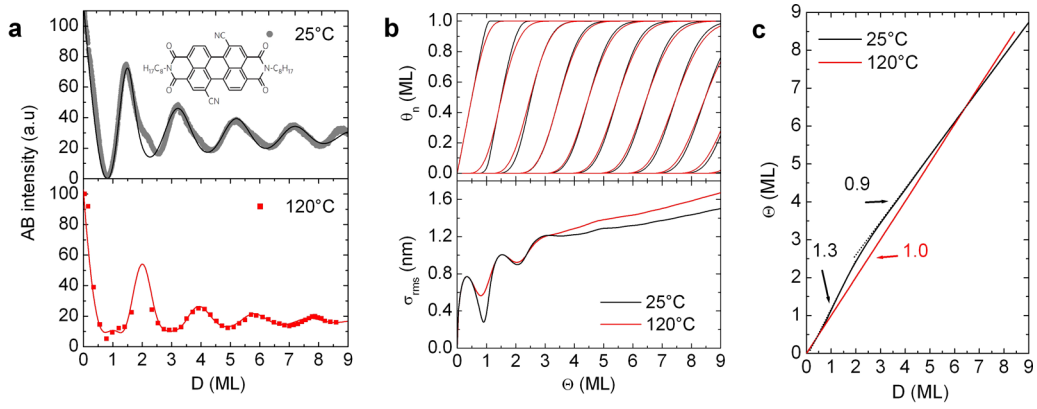

Figure 1. (a) Experimental (dots) and best fit (continuous lines) AB oscillations for T_{sub} equal to 25 and 120 °C. (b) Evolution of the θ_n (top) and σ_{rms} (bottom) *vs* total coverage Θ for T_{sub} = 25 °C (black lines) and 120 °C (red lines) extracted from the AB best fits. (c) Total coverage Θ from the fits of the AB oscillations *vs* nominal thickness D for T_{sub} = 25 °C (black line) and 120 °C (red line). The slopes of the linear segments are reported.

Here we focus on *N*,*N*′-bis(*n*-octyl)-dicyanoperylene-3,4:9,10-bis(dicarboximide) (PDI8-CN2) molecule, which is an emerging *n-type* semiconductor with high charge mobility (0.16−0.6 $cm^2\ V^{-1}\ s^{-1}$) and high ambient stability in OFET operations.[22,26,27] PDI8-CN2 does not exhibit either polymorphism[28] or thin film phases,[4,29] and hence is suitable for studying the evolution of the molecular organization during the growth of the first monolayers (MLs) in an OFET. Films of PDI8-CN2 tens of nanometers thick deposited at high substrate temperature, T_{sub}, exhibit enhanced crystallinity, morphology, and texturing, which yield an improved OFET response.[29]

Here we demonstrate that structural differences exist in the first three MLs for low (25 °C) and high (120 °C) T_{sub} and that their evolution during growth determines which ML contributes most to the charge transport in the OFET. We have used a multitechnique approach including: *in situ* real time X-ray scattering techniques, which allow us to monitor the evolution of the surface morphology at the substrate surface from the early stages of growth,[4,30−33] providing information on how MLs are filled and stacked; *in situ* real time electrical measurements which reveal the number of the active layers;[7] quantitative *ex situ* AFM which gives us insights on the growth mechanism of the first MLs.

RESULTS AND DISCUSSION

The growth dynamics is inferred from the analysis of the oscillations of X-ray reflected intensity *vs* deposition time recorded at the anti-Bragg (AB) position $q_{AB} = \pi/d$ where d is the interlayer spacing. For PDI8-CN2 films, *ex-situ* X-ray diffraction (XRD) on thin films (thickness from 5 to 50 monolayers) reveals that molecules are oriented with their long axis almost normal to the surface (edge-on configuration), and $d \approx 2$ nm.[29]

In a kinematic approximation the scattering intensity at the AB position reads[31−34]

$$I_{AB}(t) = |A_{sub}e^{i\varphi} + A_{film}\sum_{n=1}^{\infty}\theta_n(t)e^{in\pi}|^2 \qquad (1)$$

Here A_{sub} and A_{film} are the scattering amplitudes of the substrate and of the molecular monolayer, φ is the relative phase between waves scattered from substrate and molecular adlayer, θ_n is the molecular coverage of the *n*th monolayer ($\theta_n = 0$ for an empty layer, $\theta_n = 1$ for full layer). Equation 1 shows clearly that the contributions of odd and even layers have opposite sign, odd layers interfering destructively and even layers constructively (assuming $\varphi = 0$). At the completion of each θ_n the intensity exhibits minima or maxima. The oscillation intensity is modulated by the evolution of θ_n that we describe using the Trofimov model.[31,33−37]

We first plot the AB intensity *vs* the nominal thickness *D* which is directly read from the quartz microbalance.[38] From the fit $D = t\Phi$ the molecular flux Φ can be extracted. Plotting the relevant observables *vs D* instead of the time *t* allows us to compare different deposition temperatures which might change the effective deposition rate. From the fit of the AB intensity *vs D* using the Trofimov model, we extract the evolution of the molecular coverages θ_n, which yields the total coverage $\Theta = \sum_{n=1}^{\infty}\theta_n$. A calibration curve of the effective thickness, expressed as total coverage Θ in MLs, *vs D* can be constructed.

Figure 1a shows the experimental AB oscillations (dots) normalized to the maximum intensity *vs D*. The best fit (continuous lines), obtained with Supporting Information eqs 1 and 2 and the parameters reported in Supporting Information Table 1, result in a good agreement with the exception of the first peak. The fact that identical parameters have been obtained by the simultaneous fitting of the intensity oscillations recorded at different q_z values validates the model adopted (Supporting Information, Figure SI1).

In Figure 1b (top) we show the evolution of the θ_n obtained from the best fit vs Θ. At both T_{sub} the sublinear trend of θ_n just above zero or in the proximity of 1 indicates the slight deviation from the ideal layer-by-layer growth mode. At 120 °C the deviation

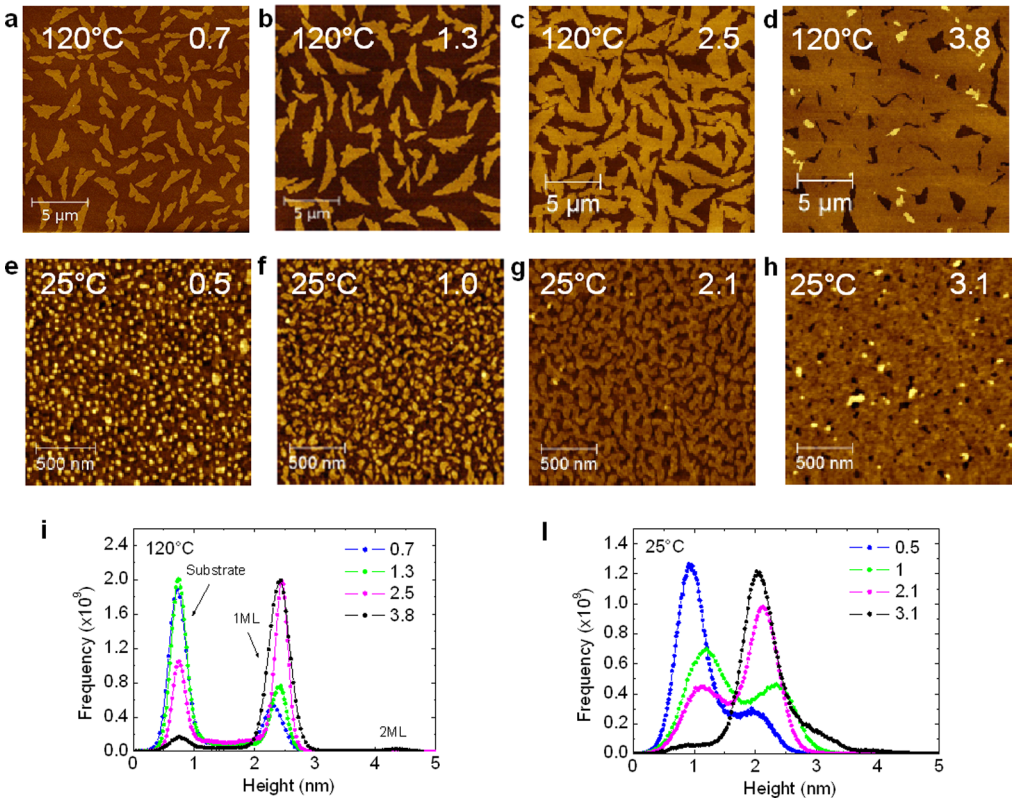

Figure 2. AFM images acquired for PDI8-CN2 films of sub-ML thickness deposited at T_{sub} = 120 °C (a−d) and at T_{sub} = 25 °C (e−h). The image labels (×10^6) are the nominal molecular density *per* μm^2; the height distributions from AFM images of the thin films deposited at T_{sub} = (i) 120 °C and (l) 25 °C.

from the ideal layer-by-layer growth is observed already at the first monolayer and is even more pronounced at the second monolayer with respect to the curves at 25 °C. These difference can be well represented from the evolution of root-mean-square roughness, σ_{rms}, which has been determined from the fitting of the AB oscillations.[33] The minima of the σ_{rms} oscillations in Figure 1b (bottom) correspond to the completion of a ML and the maxima to half ML, as typical of layer-by-layer growth. The smaller amplitude oscillation at 120 °C confirms the more marked deviation from the ideal layer-by-layer growth. Above 3 MLs the oscillations are damped and σ_{rms} scales almost linearly *vs* thickness with a larger slope for the higher T_{sub}.

In Figure 1c we plot the actual film thickness as a function of *D*. At 25 °C the growth of the first two MLs is 1.3 ± 0.1 times faster than that of following ones. The growth speed for upper layers matches, within the accuracy of the data, that at 120 °C which is constant during the deposition. The apparent acceleration of growth, reported also in thicker organic films,[35] hints to a lower density of the first MLs deposited at 25 °C.[29] For the sake of completeness, we mention that there could be a contribution from molecular desorption, more pronounced at 120 °C.

To test this hypothesis, we acquired AFM images of ultrathin films grown on thermal SiO_2/Si whose thickness was up to ∼1 ML upon identical experimental conditions of the *in situ* experiments. The latter films were labeled by the amount of molecules that impinged on the quartz microbalance. Figure 2 shows the AFM images at 120 °C (a−d) and 25 °C (e−h).

A clear T_{sub} dependence of the film morphology, as reported for thicker PDI8-CN2 films,[29] is observed: elongated islands few micrometers long and grains a few nanometers diameter form at 120 °C and at 25 °C, respectively. To complete the first ML at 120 °C a larger amount of molecules (3.8 × 10^6 molecules/μm^2) is required with respect to 25 °C (3.1 × 10^6 molecules/μm^2). This is consistent with the apparent growth acceleration estimated at 25 °C by the *in situ* X-ray scattering analysis. The nucleation of the second ML occurs when $\theta_1 \approx 0.8$ ML at 120 °C (Figure 2d) and $\theta_1 \approx 0.95$ ML at 25 °C (Figure 2h), consistently with the marked deviation from layer-by-layer growth at high T_{sub}.

The analysis of the height distribution derived from the AFM images allows us to elucidate the evolution of the molecular arrangement of the first ML. At 120 °C (Figure 2i) two sharp peaks are observed: the first peak at 0.7 nm is contributed by the substrate and the peak at ∼1.8 nm above is associated with the standing-up PDI8-CN2 molecules (*edge-on*) forming islands. When the first ML is complete, the integrated area of the first peak (substrate) decreases, whereas that of the second peak (first ML) increases. The thickest film exhibits a third peak at ∼3.8 nm above the first one, which marks

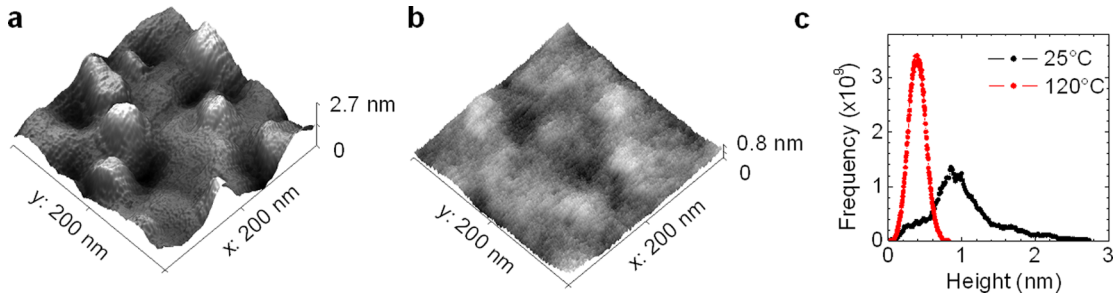

Figure 3. HR-AFM images collected on the substrate region of ultrathin films grown (a) at 25 °C and (b) 120 °C; (c) height distributions extracted from images a and b.

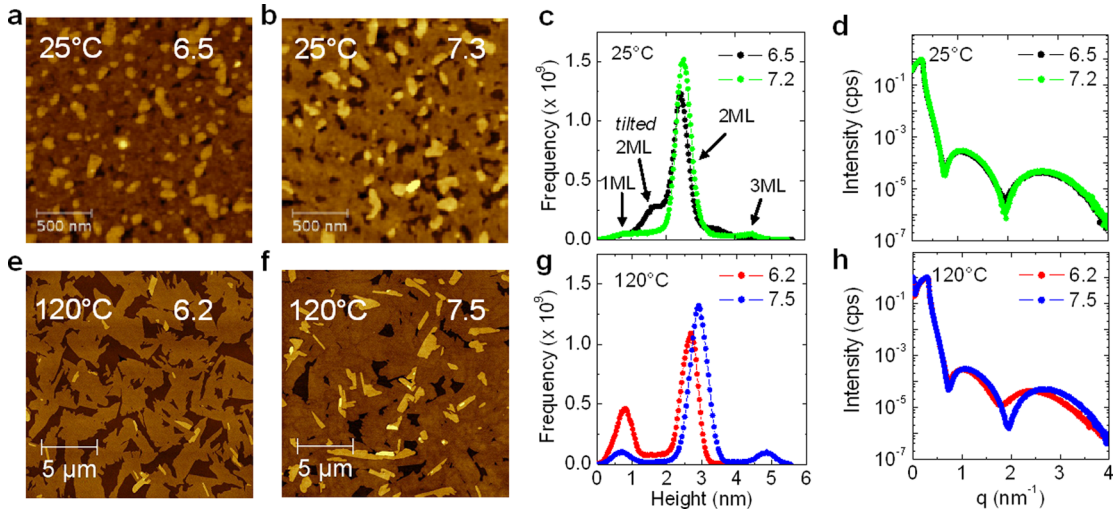

Figure 4. AFM images of films deposited with nominal density of (a,e) ~6 × 10^6 molecules/μm^2 and (b,f) ~7 × 10^6 molecules/μm^2, at 25 and 120 °C; (c,g) the corresponding height distributions and (d,h) XRR curves.

the growth of the second ML where molecules exhibit the same orientation of the first monolayer.

The same trend is observed at 25 °C (Figure 2l) but the broadening of the first peak at 0.9 nm indicates an increased substrate roughness. This can be ascribed to a spatially inhomogeneous distribution of molecular mounds formed by face-on or bent/distorted edge-on molecules. By associating the second peak with the edge-on molecules forming islands, the separation between the two peaks (~1.1 nm) is smaller than that observed at 120 °C. It can be explained by the presence of these inhomogeneous molecular mounds between islands. The coexistence of flat-lying molecules on the substrate was reported earlier for sexithienyl.[24,39]

Figure 3a,b show high-resolution AFM images, recorded with amplitude modulation mode in attractive regime,[40] of a region between islands of standing molecules in submonolayer films grown with a low nominal molecular density (0.5 × 10^6 and 0.7 × 10^6 molecules/μm^2 at 25 and 120 °C respectively). The topography at 25 °C (Figure 3a) is inhomogeneous due to the presence of aggregates thinner than 2 nm; they contribute several peaks to the histogram in Figure 3c, the main peak centered at ~0.9 nm, that is, ~0.5 nm above the bare substrate. This value is consistent with molecules lying flat on the substrate. The shoulder to the larger height side of the main peak confirms the coexistence of several configurations of the molecules lying on the substrate. Conversely, the topography at 120 °C (Figure 3b) is flat and its height distribution exhibits only the symmetrical peak ascribed to the bare substrate roughness (~0.4 nm).

To follow the progressive molecular arrangement we have assessed the topography from AFM images (Figure 4) of thicker films (~2MLs) obtained by depositing ~6 × 10^6 (a,e) and ~7 × 10^6 molecules/μm^2 (b,f) at the two T_{sub}.

At low T_{sub} upon an increase of nominal density by 1.1 × 10^6 molecules/μm^2, the morphology of the films appears unchanged (Figure 4a,b). However, the height distribution (Figure 4c) reveals the coexistence of two populations with different molecular orientation in the second ML: the weaker peak, 0.8 nm above the first ML, is related to the minority population of tilted/bent molecules; the stronger, ~1.8 nm above the first ML, to the majority population. By increasing the thickness, the weaker peak disappears in favor of the stronger one indicating a rearrangement of the tilted/bent molecules of the second ML into a more stable configuration with standing molecules. A similar phenomenon is

observed also for the molecules on the third ML, the height of which shifts from 2.7 nm (at 6.2 × 10^6 molecules/μm^2) to 3.7 nm (at 7.3 × 10^6 molecules/μm^2) above the first ML. The X-ray reflectivity (XRR) curves of the two samples are surprisingly similar (Figure 4d); their analysis[41] evidences the same film thickness (4.4 ± 0.1 nm, corresponding to ~2MLs of molecules in edge-on configuration) and roughness (0.4 ± 0.1 nm) with only a slight difference of mass density (1.02 ± 0.02 g/cm^3 for 6.2 × 10^6 molecules/μm^2 and 1.13 ± 0.02 g/cm^3 for 7.3 × 10^6 molecules/μm^2). The thickness value corresponds to the most intense peak in the height distribution in Figure 4c, which indicates that the majority of the molecules of the second ML stand up. The increased density of the thicker film is consistent with a closer packed molecular configuration. For the sake of clarity, we proved that XRR curves cannot be fitted by the same mass density, even releasing the other parameters (Supporting Information, Figure SI2).

The evolution of the films deposited at 120 °C (Figure 4e,f) can be explained by the completion of the second ML followed by nucleation and growth of the third one. The height distributions (Figure 4g) indicate that the molecules of the second ML evolve only slightly to reach a more stable configuration. The analysis of XRR curves (Figure 4h) indicates a roughness decreasing due to the completion of the second ML.

Interestingly, the mass density of the film ~2MLs thick (~ 6 × 10^6 molecules/μm^2) at 25 °C (1.02 g/cm^3) is lower than that at 120 °C (1.49 ± 0.02 g/cm^3) (see Supporting Information, Figure SI3). This confirms that, although at both T_{sub} the crystallites are formed by PDI8-CN2 molecules standing up on the substrate, at 25 °C the molecular packing, averaged over the first two MLs, is less dense than that at 120 °C. The difference in mass density at the two T_{sub} disappears when the film thickness is greater than 3MLs, as reported in Supporting Information, Figure SI4. This confirms the fact that the molecular orientation/configuration differs for the two T_{sub} just in the first MLs closer to the substrate. This has substantial consequences on the charge transport in a field-effect transistor when an ultrathin film is deposited, as discussed later. Although molecular reorganization takes place during the growth at 25 °C, in thicker films a crystalline order lower than the film grown at 120 °C is evidenced by XRD measurements (see Supporting Information, Figure SI5a,b).

The presence of the edge-on/bent molecules at 25 °C demonstrates the lower layer density inferred upon fitting the AB oscillations. Density variation modifies the scattering amplitude of the first MLs, which instead is kept fixed in the Trofimov model. This approximation could justify why the shoulder appearing in the first oscillation around 2MLs of nominal thickness is not well reproduced. The maximum of the AB oscillation at around 1.6 MLs of nominal thickness could correspond to the complete coverage of the second monolayer with the coexistence of different molecular configuration; the shoulder at 2 ML of nominal thickness could correspond to the second completion of the second monolayer, where most of defects heal before the nucleation of the third monolayer.

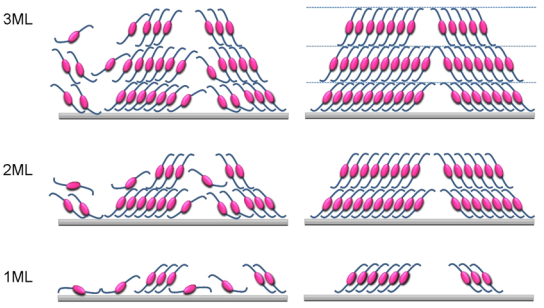

Figure 5. Schematic representation of PDI8-CN2 growth at 25 °C (left) and 120 °C (right).

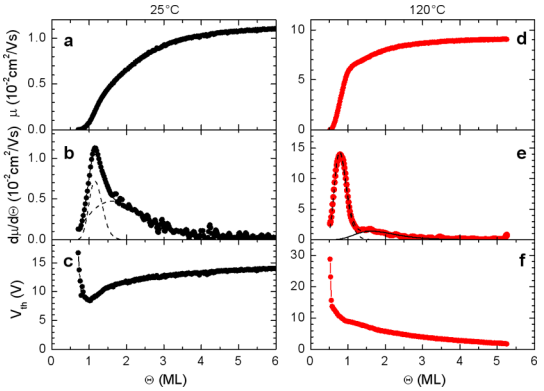

Figure 6. Evolution of OFET properties *vs* thickness for thin films grown at 25 °C (a−c) and 120 °C (d−f). (a,d) Charge mobility μ_{lin} extracted from the transfer characteristics in the linear regime; (b,e) first derivative of μ_{lin} (dots) and its best-fit (continuous black line) obtained by linear combination of two log-normal functions (dashed lines); (c,f) threshold voltage.

The emerging scenario is schematically depicted in Figure 5. At 25 °C stable and metastable configurations coexist at the early stages of growth, then metastable molecular domains reorganize within each monolayer as the growth proceeds, increasing the size of stable crystalline phase domains. The coexistence of domains with different molecular configuration in the first monolayers at 25 °C represents a defect that dynamically heals, albeit not completely. At 120 °C the film grows in the more stable crystalline phase[29] from the early stages, with only a slight rearrangement of edge-on molecules.

We assess the impact of the presence of these dynamic defects on the charge distribution and the transport properties of a field effect transistor by monitoring *in situ* and in real time the evolution of the charge mobility μ during the growth. The trends of μ_{lin} *vs* thickness extracted in the linear regime from the transfer characteristics are shown in Figure 6a,d. The values μ_{sat} in the saturation regime are shown in

Supporting Information, Figure SI6. The charge mobility at 120 °C is one order of magnitude larger than that evaluated at 25 °C, as already observed in the *ex situ* measurements on thicker PDI8-CN2 films,[29] consistent with higher crystallinity, lower occurrence of grain boundaries and highly uniform molecular organization at high T_{sub}.

From the analysis of μ_{lin} evolution, information on the charge transport mechanism is obtained. The percolation coverage Θ_p at which the current I_{DS} becomes detectable above the noise level is dependent on T_{sub}: $\Theta_p = 0.7$ ML at $T_{sub} = 25$ °C and $\Theta_p = 0.5$ ML at $T_{sub} = 120$ °C. In the percolation theory,[42,43] Θ_p marks the appearance of the first connected percolation path between source and drain. The values found are in agreement with the percolation theory which predicts that Θ_p attains the value of 0.67 ML for 2D percolation between grains with isotropic shape (as those at 25 °C). It is expected that Θ_p varies slightly with the grain sizes and decreases as the aspect ratio of anisotropic grains (as those at 120 °C) increases.[44] Above Θ_p, μ_{lin} increases with the film thickness in a different manner for the two T_{sub}. At 25 °C (Figure 6a) it increases continuously up to a saturation value of 0.01 $cm^2/(V\ s)$ for $\Theta > 4$ MLs. At 120 °C (Figure 6d) it increases to 0.06 $cm^2/(V\ s)$ when the first monolayer completes. After the inflection point at 1.5 MLs, it slowly reaches a saturation value of 0.1 $cm^2/(V\ s)$ in the following 3 MLs. The latter trend is even more marked in the saturation regime (Supporting Information, Figure SI6). The analysis of the derivative of μ_{lin} with respect to the film thickness, $d\mu_{lin}/d\Theta$, allows us to infer the contributions of the different monolayers to the charge mobility. As a first approximation, the first derivative scales as the charge carrier density.[45] Figure 6b,e shows experimental $d\mu_{lin}/d\Theta$ curves (dots) and their best fit curves (continuous lines) obtained by using a linear combination of two log-normal functions (dashed lines), as detailed earlier.[7] At 120 °C, the derivative exhibits two well separated peaks at ~1 ML and ~2 ML thickness. This clearly shows that the charge density is confined to the first two MLs, and that each monolayer acts as an independent channel for 2D charge transport. The main contribution, estimated from the integral area of the peak (75%), is from the first monolayer. At 25 °C the first peak is still sharp, whereas the second peak is broad, overlaps with the first peak, and spans up to several MLs. Interestingly, the main contribution (80%) comes from the second peak. This shows that the inhomogeneous molecular arrangement of the first monolayers prevents efficient charge accumulation and transport. The molecular reorganization occurring during growth heals the inhomogeneity and this reflects itself in the dominant contribution from the broad peak. If we compare the effective Debye length, defined as the maximum thickness where 63% of the maximum mobility[7] is contributed, we notice that it equals 1 ML for $T_{sub} = 120$ °C and is greater than 2 MLs for $T_{sub} = 25$ °C. Despite this reorganization, the crystalline order at 25 °C is lower than that of the film grown at 120 °C. This causes the charge mobility of the thicker film at 25 °C also to be lower.

The threshold voltage (Figure 6 c,f) is positive, and as the thin film grows it decreases from the initial value to reach a plateau of 14 V at 25 °C and 0 V at 120 °C. As the film grows, fewer trap states for electrons need to be compensated before the transistor turns on. This trend is similar (although in the opposite direction being here an n-type semiconductor) to that observed on pentacene FETs.[46] The different limits at the two temperatures indicate that the shallow traps are located in the first monolayers of the thin film. The residual threshold voltage in the case of 25 °C reflects the incomplete healing of the molecular disorder of the first MLs.

As reported for other molecular semiconductors,[1,7] the effective Debye length in stacked molecular thin films is limited by the discontinuity of the upper layers, rather than by the screening of the transversal electric field. In rod-like oligomer thin films, a roughening transition occurs at about 1−2 ML coverage, leading to a change from layer-by-layer to island growth. The upper layers, albeit populated, do not effectively contribute to charge transport.

Here we have demonstrated that, in spite of the marginal difference in the growth mode of PDI8-CN2 films at different T_{sub}, a marked difference in the molecular density of the first few MLs occurs. At 25 °C the coexistence of domains with different molecular orientations in the first MLs yields lower dielectric permittivity and charge mobility. This effect is partially compensated by the molecular reorganization toward homogeneously ordered monolayers which, however, stops at the completion of the third ML. Because the energy barriers for molecular reorganization of the second and third ML should be lower than those of the first one, the upper layers "heal" more rapidly and extensively than the first ML. This may cause their dominant contribution to charge transport, and the monotonic increase of μ_{lin} until saturation is attained above 3 MLs.

CONCLUSIONS

We have demonstrated that PDI8-CN2, grown in a quasi layer-by-layer mode at two different substrate temperatures, exhibits a marked difference in molecular organization, crystal order, and density, which also reflects in the distribution of charge carriers in a transistor. We have elucidated the nature of orientational defects at 25 °C, consisting of coexisting domains with either standing molecules or planar/tilted/bent molecules in the first PDI8-CN2 monolayers at the gate dielectric interface in working devices. Although these defects tend to heal dynamically, their formation at the early stages has an impact on the charge transport

properties of the device: they are the cause of depletion of charge carriers in the first monolayer, leading to the second monolayer being dominant in charge transport. This suggests that the defects effectively behave as shallow traps for electrons.

Conversely, at 120 °C the trend of charge mobility *vs* thickness is consistent with ideal 2D charge transport, where electron percolation occurs within each monolayer and no substantial charge transfer between adjacent monolayers occurs. In this case most of the charge carrier density is in the first monolayer. This highlights the complexity of the growth phenomena and their subtle effects on the device response, and how their control is technologically challenging.

EXPERIMENTAL METHODS

Materials. PDI8-CN2 molecules were used as received from BASF.

***In Situ* and Real Time Measurements.** Structural and electrical characterizations have been performed *in situ* and in real time during HV deposition of PDI8-CN2 thin film on bare SiO_2/Si wafers and on FET test patterns, respectively. The molecular flux Φ has been chosen ~0.1 ML/min, where 1 ML, defined by the d_{001} spacing, is approximately equal to 2 nm. This low flux minimizes the variation of the thin-film thickness between the beginning and the end of each characterization measurement and it enables real time investigations to be performed continuously, without interrupting the deposition. Depositions at low (25 °C) and high (120 °C) T_{sub} have been compared.

X-ray scattered intensities have been recorded in specular configuration at anti-Bragg (AB) position q_{AB} in an in-house developed HV chamber (baseline pressure P $\approx 10^{-8}$ mbar)[47] designed to be compatible with *in situ* X-ray measurements. The chamber was installed on the 6-circle diffractometer at beamline ID10B at the ESRF (Grenoble-France). The X-ray energy was fixed at 13.68 keV and the maximum counting time was 120 s; at least 10 points have been recorded for each ML.

After each deposition 2D-GID images were collected using an incident angle of the X-ray beam, α_i, close to the critical angle for total reflection of the organic film (*i.e.*, 0.13°). The diffraction patterns were recorded by an in-plane scan of a linear detector oriented normal to the incident beam direction and equipped with soller slits ($\Delta\alpha = 0.08°$).

The test patterns (Fondazione Bruno Kessler, Trento, Italy)[7] used for the electrical studies have channel lengths of 20 and 40 μm, and a width of 11200 and 22400 μm, respectively. Drain and source Au (150 nm)/Cr (3−5 nm) electrodes are lithographically defined on a 200 nm thick SiO_2 film thermally grown on highly doped *n*-type Si wafer which acts as common gate electrode. Before deposition, the test patterns have been cleaned with Piranha solution (1:1 H_2O_2/H_2SO_4) for 15 min and in 4% HF solution for a few seconds. This procedure removes Cr at the boundary between the electrode and the channel.[48,49] The transfer characteristic, that is, source−drain current, I_{DS} *vs* applied gate-source bias, V_{GS}, has been measured in linear and saturation regimes (with V_{DS} = 5 V and V_{DS} = 30 V, respectively) sweeping V_{GS} continuously between +50 V and −30 V (forward and backward sweep) with a 1 V step. For each V_{GS} value I_{DS} has been measured with an integration time of 20 ms, corresponding to 1.6 s to record a complete transfer curve.

For each T_{sub} four devices have been measured, two in the linear and two in the saturation regime.

***Ex Situ* Measurements.** A series of ultrathin films (from 0.5 to 3 ML) deposited on SiO_2/Si, exactly in the same conditions reported above, have been characterized after deposition. The morphology has been studied by collecting AFM images in air in semicontact mode using a Smena NT-MDT microscope equipped with NSG10 cantilevers. The film thickness has been reported as the function of the amount of molecules deposited on the quartz microbalance.

Structural characterization by X-ray reflectivity measurements has been performed with a SmartLab-Rigaku diffractometer equipped with a rotating anode (Cu Kα, λ = 0.154 nm), followed by a parabolic mirror to collimate the incident beam, and a series of variable slits (placed before and after the sample position). XRD data in out-of-plane specular geometry have been recorded for selected thick films at beamline ID10B at the ESRF (Grenoble-France), with the X-ray energy fixed at 13.45 keV and defined by two vertical slits before a linear detector rotating around the normal axis of the film surface.

Conflict of Interest: The authors declare no competing financial interest.

Acknowledgment. We are grateful to Dr. Silke Kohler (BASF, Ludswigshafen) for supplying us PDI8-CN2, Dr. Otello M. Roscioni (Alma Mater Studiorum-Università di Bologna) for stimulating discussions, and Dr. Oleg Konovalov for his help and suggestions during the experiment performed at ESRF. This work was supported by the EU Large Project One-P (FP7-NMP-2007-212311) and by DFG.

Supporting Information Available: AB, XRR, and XRD data analysis and *in situ* and real time electrical measurements performed in saturation regime. This material is available free of charge *via* the Internet at http://pubs.acs.org.

REFERENCES AND NOTES

1. Dinelli, F.; Murgia, M.; Levy, P.; Cavallini, M.; Biscarini, F.; de Leeuw, D. M. Spatially Correlated Charge Transport in Organic Thin Film Transistors. *Phys. Rev. Lett.* **2004**, *92*, 116802.
2. Muck, T.; Wagner, V.; Bass, U.; Leufgen, M.; Geurts, J.; Molenkamp, L. W. *In Situ* Electrical Characterization of DH4T Field-Effect Transistors. *Synth. Met.* **2004**, *146*, 317–320.
3. Gomes, H. L.; Stallinga, P.; Colle, M.; de Leeuw, D. M.; Biscarini, F. Electrical Instabilities in Organic Semiconductors Caused by Trapped Supercooled Water. *Appl. Phys. Lett.* **2006**, *88*, 082101.
4. Ruiz, R.; Mayer, A. C.; Malliaras, G. G.; Nickel, B.; Scoles, G.; Kazimirov, A.; Kim, H.; Headrick, R. L.; Islam, Z. Structure of Pentacene Thin Films. *Appl. Phys. Lett.* **2004**, *85*, 4926–4928.
5. Kiguchi, M.; Nakayama, M.; Shimada, T.; Saiki, K. Electric-Field-Induced Charge Injection or Exhaustion in Organic Thin Film Transistor. *Phys. Rev. B* **2005**, *71*, 035332.
6. Park, B. N.; Seo, S.; Evans, P. G. Channel Formation in Single-Monolayer Pentacene Thin Film Transistors. *J. Phys. D* **2007**, *40*, 3506–3511.
7. Shehu, A.; Quiroga, S. D.; D'Angelo, P.; Albonetti, C.; Borgatti, F.; Murgia, M.; Scorzoni, A.; Stoliar, P.; Biscarini, F. Layered Distribution of Charge Carriers in Organic Thin Film Transistors. *Phys. Rev. Lett.* **2010**, *104*, 246602.
8. Brondijk, J. J.; Roelofs, W. S. C.; Mathijssen, S. G. J.; Shehu, A.; Cramer, T.; Biscarini, F.; Blom, P. W. M.; de Leeuw, D. M. Two-Dimensional Charge Transport in Disordered Organic Semiconductors. *Phys. Rev. Lett.* **2012**, *109*, 056601.
9. Verlaak, S.; Steudel, S.; Heremans, P.; Janssen, D.; Deleuze, M. S. Nucleation of Organic Semiconductors on Inert Substrates. *Phys. Rev. B* **2003**, *68*, 195409.
10. Markov, I. V. *Crystal Growth for Beginners: Fundamentals of Nucleation, Crystal Growth and Epitaxy*; World Scientific: Singapore, 1995.
11. Gotzen, J.; Schwalb, C. H.; Schmidt, C.; Mette, G.; Marks, M.; Hofer, U.; Witte, G. Structural Evolution of Perfluoro-Pentacene Films on Ag(111): Transition from 2D to 3D Growth. *Langmuir* **2011**, *27*, 993–999.

12. Mayer, A. C.; Kazimirov, A.; Malliaras, G. G. Dynamics of Bimodal Growth in Pentacene Thin Films. *Phys. Rev. Lett.* **2006**, *97*, 105503.
13. Biscarini, F.; Zamboni, R.; Samori, P.; Ostoja, P.; Taliani, C. Growth of Conjugated Oligomer Thin-Films Studied by Atomic-Force Microscopy. *Phys. Rev. B* **1995**, *52*, 14868–14877.
14. Biscarini, F.; Samori, P.; Greco, O.; Zamboni, R. Scaling Behavior of Anisotropic Organic Thin Films Grown in High Vacuum. *Phys. Rev. Lett.* **1997**, *78*, 2389–2392.
15. Melucci, M.; Gazzano, M.; Barbarella, G.; Cavallini, M.; Biscarini, F.; Maccagnani, P.; Ostoja, P. Multiscale Self-Organization of the Organic Semiconductor Alpha-Quinquethiophene. *J. Am. Chem. Soc.* **2003**, *125*, 10266–10274.
16. Cicoira, F.; Santato, C.; Dinelli, F.; Murgia, M.; Loi, M. A.; Biscarini, F.; Zamboni, R.; Heremans, P.; Muccini, M. Correlation between Morphology and Field-Effect-Transistor Mobility in Tetracene Thin Films. *Adv. Funct. Mater.* **2005**, *15*, 375–380.
17. Hlawacek, G.; Puschnig, P.; Frank, P.; Winkler, A.; Ambrosch-Draxl, C.; Teichert, C. Characterization of Step-Edge Barriers in Organic Thin-Film Growth. *Science* **2008**, *321*, 108–111.
18. Zhang, X. N.; Barrena, E.; Goswami, D.; de Oteyza, D. G.; Weis, C.; Dosch, H. Evidence for a Layer-Dependent Ehrlich−Schwobel Barrier in Organic Thin Film Growth. *Phys. Rev. Lett.* **2009**, *103*, 136101.
19. Woll, C. *Physical and Chemical Aspects of Organic Electronics*; Wiley-VHC: Weinheim, 2009.
20. Ohashi, N.; Tomii, H.; Matsubara, R.; Sakai, M.; Kudo, K.; Nakamura, M. Conductivity Fluctuation within a Crystalline Domain and its Origin in Pentacene Thin-Film Transistors. *Appl. Phys. Lett.* **2007**, *91*, 162105.
21. Annibale, P.; Albonetti, C.; Stoliar, P.; Biscarini, F. High-Resolution Mapping of the Electrostatic Potential in Organic Thin-Film Transistors by Phase Electrostatic Force Microscopy. *J. Phys. Chem. A* **2007**, *111*, 12854–12858.
22. Rivnay, J.; Jimison, L. H.; Northrup, J. E.; Toney, M. F.; Noriega, R.; Lu, S. F.; Marks, T. J.; Facchetti, A.; Salleo, A. Large Modulation of Carrier Transport by Grain-Boundary Molecular Packing and Microstructure in Organic Thin Films. *Nat. Mater.* **2009**, *8*, 952–958.
23. Muccini, M.; Murgia, M.; Biscarini, F. Energy Transfer Tailoring in Conjugated Molecular Architectures. *Adv. Mater.* **2001**, *13*, 355–358.
24. Loi, M. A.; Da Como, E.; Dinelli, F.; Murgia, M.; Zamboni, R.; Biscarini, F.; Muccini, M. Supramolecular Organization in Ultrathin Films of Alpha-Sexithiophene on Silicon Dioxide. *Nat. Mater.* **2005**, *4*, 81–85.
25. Dinelli, F.; Moulin, J. F.; Loi, M. A.; Da Como, E.; Massi, M.; Murgia, M.; Muccini, M.; Biscarini, F.; Wie, J.; Kingshott, P. Effects of Surface Chemical Composition on the Early Growth Stages of Alpha-Sexithienyl Films on Silicon Oxide Substrates. *J. Phys. Chem. B* **2006**, *110*, 258–263.
26. Yoo, B.; Jung, T.; Basu, D.; Dodabalapur, A.; Jones, B. A.; Facchetti, A.; Wasielewski, M. R.; Marks, T. J. High-Mobility Bottom-Contact n-Channel Organic Transistors and Their Use in Complementary Ring Oscillators. *Appl. Phys. Lett.* **2006**, *88*, 082104.
27. Jones, B. A.; Facchetti, A.; Wasielewski, M. R.; Marks, T. J. Effects of Arylene Diimide Thin Film Growth Conditions on n-Channel OFET Performance. *Adv. Funct. Mater.* **2008**, *18*, 1329–1339.
28. Brillante, A.; Bilotti, I.; Albonetti, C.; Moulin, J. F.; Stoliar, P.; Biscarini, F.; de Leeuw, D. M. Confocal Raman Spectroscopy of Alpha-Sexithiophene: From Bulk Crystals to Field-Effect Transistors. *Adv. Funct. Mater.* **2007**, *17*, 3119–3127.
29. Liscio, F.; Milita, S.; Albonetti, C.; D'Angelo, P.; Guagliardi, A.; Masciocchi, N.; Della Valle, R. G.; Venuti, E.; Brillante, A.; Biscarini, F. Structure and Morphology of PDI8-CN2 for n-Type Thin-Film Transistors. *Adv. Funct. Mater.* **2012**, *22*, 943–953.
30. Krause, B.; Schreiber, F.; Dosch, H.; Pimpinelli, A.; Seeck, O. H. Temperature Dependence of the 2D−3D Transition in the Growth of PTCDA on Ag(111): A Real-Time X-ray and Kinetic Monte Carlo Study. *Europhys. Lett.* **2004**, *65*, 372–378.
31. Kowarik, S.; Gerlach, A.; Skoda, M. W. A.; Sellner, S.; Schreiber, F. Real-Time Studies of Thin Film Growth: Measurement and Analysis of X-ray Growth Oscillations beyond the anti-Bragg Point. *Eur. Phys. J-Spec. Top.* **2009**, *167*, 11–18.
32. Kowarik, S.; Gerlach, A.; Sellner, S.; Schreiber, F.; Cavalcanti, L.; Konovalov, O. Real-Time Observation of Structural and Orientational Transitions During Growth of Organic Thin Films. *Phys. Rev. Lett.* **2006**, *96*, 125504.
33. Cohen, P. I.; Petrich, G. S.; Pukite, P. R.; Whaley, G. J.; Arrott, A. S. Birth Death Models of Epitaxy 1. Diffraction Oscillations from Low Index Surfaces. *Surf. Sci.* **1989**, *216*, 222–248.
34. Woll, A. R.; Desai, T. V.; Engstrom, J. R. Quantitative Modeling of *In Situ* X-ray Reflectivity During Organic Molecule Thin Film Growth. *Phys. Rev. B* **2011**, *84*, 075479.
35. Amassian, A.; Desai, T. V.; Kowarik, S.; Hong, S.; Woll, A. R.; Malliaras, G. G.; Schreiber, F.; Engstrom, J. R. Coverage Dependent Adsorption Dynamics in Hyperthermal Organic Thin Film Growth. *J. Chem. Phys.* **2009**, *130*, 124701.
36. Trofimov, V. I.; Kim, J.; Bae, S. Influence of Two Different Adatom Mobilities on the Initial Heteroepitaxial Growth Kinetics. *Surf. Sci.* **2007**, *601*, 4465–4469.
37. Weber, C.; Frank, C.; Bommel, S.; Rukat, T.; Leitenberger, W.; Schafer, P.; Schreiber, F.; Kowarik, S. Chain-Length Dependent Growth Dynamics of *n*-Alkanes on Silica Investigated by Energy-Dispersive X-ray Reflectivity *in Situ* and in Real-Time. *J. Chem. Phys.* **2012**, *136*, 204709.
38. The thickness measured by the quartz balance has been calibrated from the XRR data collected for a thick films after deposition.
39. Dinelli, F.; Albonetti, C.; Kolosov, O. V. Ultrasonic Force Microscopy: Detection and Imaging of Ultrathin Molecular Domains. *Ultramicroscopy* **2011**, *111*, 267–272.
40. Garcia, R.; Perez, R. Dynamic Atomic Force Microscopy Methods. *Surf. Sci. Rep.* **2002**, *47*, 197–301.
41. Colombi, P.; Agnihotri, D. K.; Asadchikov, V. E.; Bontempi, E.; Bowen, D. K.; Chang, C. H.; Depero, L. E.; Farnworth, M.; Fujimoto, T.; Gibaud, A.; *et al.* Reproducibility in X-ray Reflectometry: Results from the First World-Wide Round-Robin Experiment. *J. Appl. Crystallogr.* **2008**, *41*, 143–152.
42. Sreenivasan, S.; Baker, D. R.; Paul, G.; Stanley, H. E. The Approximate Invariance of the Average Number of Connections for the Continuum Percolation of Squares at Criticality. *Phys. A* **2003**, *320*, 34–40.
43. Quintanilla, J.; Torquato, S.; Ziff, R. M. Efficient Measurement of the Percolation Threshold for Fully Penetrable Discs. *J. Phys A, Math. Gen.* **2000**, *33*, L399–L407.
44. Garboczi, E. J.; Snyder, K. A.; Douglas, J. F.; Thorpe, M. F. Geometrical Percolation-Threshold of Overlapping Ellipsoids. *Phys. Rev. E* **1995**, *52*, 819–828.
45. Tanase, C.; Meijer, E. J.; Blom, P. W. M.; de Leeuw, D. M. Local Charge Carrier Mobility in Disordered Organic Field-Effect Transistors. *Org. Electron.* **2003**, *4*, 33–37.
46. Fiebig, M.; Beckmeier, D.; Nickel, B. Thickness-Dependent *in Situ* Studies of Trap States in Pentacene Thin Film Transistors. *Appl. Phys. Lett.* **2010**, *96*, 083304.
47. Durr, A. C.; Schreiber, F.; Ritley, K. A.; Kruppa, V.; Krug, J.; Dosch, H.; Struth, B. Rapid Roughening in Thin Film Growth of an Organic Semiconductor (Diindenoperylene). *Phys. Rev. Lett.* **2003**, *90*, 647.
48. Williams, K. R.; Gupta, K.; Wasilik, M. Etch Rates for Micromachining Processing—Part II. *J. Microelectromech. Syst.* **2003**, *12*, 761–778.
49. Mathijssen, S. G. J.; Smits, E. C. P.; van Hal, P. A.; Wondergem, H. J.; Ponomarenko, S. A.; Moser, A.; Resel, R.; Bobbert, P. A.; Kemerink, M.; Janssen, R. A. J.; *et al.* Monolayer Coverage and Channel Length Set the Mobility in Self-Assembled Monolayer Field-Effect Transistors. *Nat. Nanotechnol.* **2009**, *4*, 674–680.